AMERICAN SOCIETY FOR MICROBIOLOGY | Journal of Virology®

STRUCTURE AND ASSEMBLY

Antibody Recognition of CD4-Induced Open HIV-1 Env Trimers

Zhi Yang,[a] Kim-Marie A. Dam,[a] Jonathan M. Gershoni,[b] Susan Zolla-Pazner,[c] Pamela J. Bjorkman[a]

[a]Division of Biology and Biological Engineering, California Institute of Technology, Pasadena, California, USA
[b]Shmunis School of Biomedicine and Cancer Research, Tel Aviv University, Tel Aviv, Israel
[c]Department of Medicine, Division of Infectious Diseases, Icahn School of Medicine at Mount Sinai, New York, New York, USA

Zhi Yang and Kim-Marie A. Dam contributed equally to this work and are co-first authors. Author order was determined by them.

ABSTRACT Human immunodeficiency virus type 1 (HIV-1) envelope (Env), a heterotrimer of gp120-gp41 subunits, mediates fusion of the viral and host cell membranes after interactions with the host receptor CD4 and a coreceptor. CD4 binding induces rearrangements in Env trimer, resulting in a CD4-induced (CD4i) open Env conformation. Structural studies of antibodies isolated from infected donors have defined antibody-Env interactions, with one class of antibodies specifically recognizing the CD4i open Env conformation. In this study, we characterized a group of monoclonal antibodies isolated from HIV-1 infected donors (V2i MAbs) that displayed characteristics of CD4i antibodies. Binding experiments demonstrated that the V2i MAbs preferentially recognize CD4-bound open Env trimers. Structural characterizations of V2i MAb-Env-CD4 trimer complexes using single-particle cryo-electron microscopy showed recognition by V2i MAbs using different angles of approach to the gp120 V1V2 domain and the $\beta2/\beta3$ strands on a CD4i open conformation Env with no direct interactions of the MAbs with CD4. We also characterized CG10, a CD4i antibody that was raised in mice immunized with a gp120-CD4 complex, bound to an Env trimer plus CD4. CG10 exhibited characteristics similar to those of the V2i antibodies, i.e., recognition of the open Env conformation, but showed direct contacts to both CD4 and gp120. Structural comparisons of these and previously characterized CD4i antibody interactions with Env provide a suggested mechanism for how these antibodies are elicited during HIV-1 infection.

IMPORTANCE The RV144 HIV-1 clinical vaccination trial showed modest protection against viral infection. Antibody responses to the V1V2 region of HIV-1 Env gp120 were correlated inversely with the risk of infection, and data from three other clinical vaccine trials suggested a similar signal. In addition, antibodies targeting V1V2 have been correlated with protections from simian immunodeficiency virus (SIV) and simian-human immunodeficiency virus (SHIV) infections in nonhuman primates. We structurally characterized V2i antibodies directed against V1V2 isolated from HIV-1 infected humans in complex with open Env trimers bound to the host receptor CD4. We also characterized a CD4i antibody that interacts with CD4 as well as the gp120 subunit of an open Env trimer. Our study suggests how V2i and CD4i antibodies were elicited during HIV-1 infection.

KEYWORDS CD4i antibody, CG10 antibody, HIV-1 Env, V2i MAb, monoclonal antibodies

The HIV-1 envelope glycoprotein (Env), the only viral protein on the surface of the virus, interacts with target cells to mediate fusion between the viral and host cell membranes, a process that marks the initiation of HIV-1 infection (1–3). The trimeric Env is composed of three copies of gp120-gp41 heterodimers (1). To infect cells, the gp120 subunit interacts with the host cell receptor CD4 and undergoes a series of conformational changes that lead to the exposure of the binding site for a host cell coreceptor, either CCR5 or CXCR4 (4, 5). Env binding to its coreceptor results in further

Editor Viviana Simon, Icahn School of Medicine at Mount Sinai

Address correspondence to Pamela J. Bjorkman, bjorkman@caltech.edu.

The authors declare no conflict of interest.

Received 12 July 2022
Accepted 11 October 2022
Published 30 November 2022

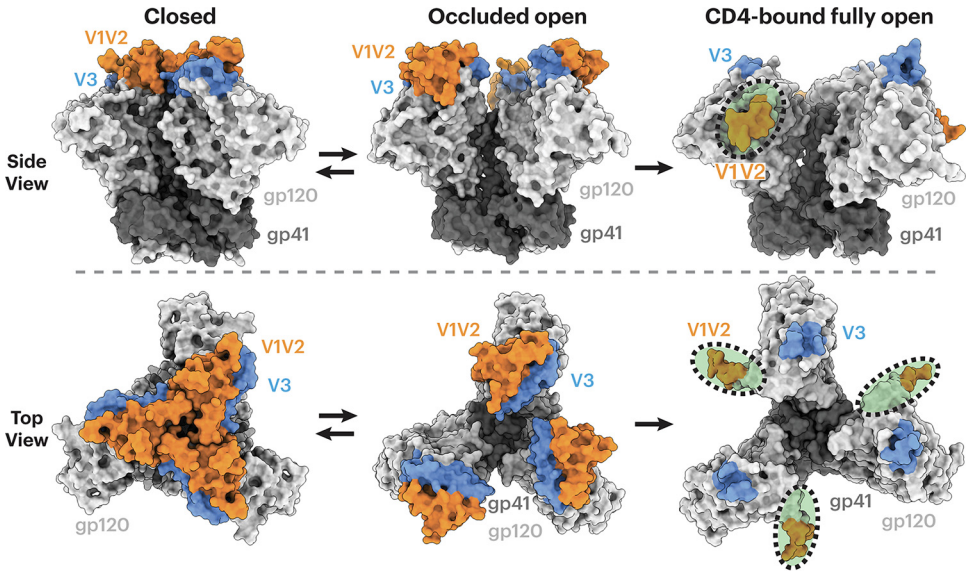

FIG 1 HIV Env trimers can adopt several conformational states. Env gp120 subunits are light gray, gp41 is dark gray, V1V2 regions are orange, and V3 is blue. HIV-1 Envs in different conformational states are shown in side (top) or top (bottom) views. (Left) Closed, prefusion Env trimer conformation with gp120 V1V2 at the apex of the trimer (PDB code 5CEZ); (middle) occluded open conformation with outwardly rotated gp120 protomers but no local structural rearrangements in V1V2 or V3 (PDB code 7TFN); (right) CD4-bound fully open conformation (sCD4 not shown) with V1V2 regions largely disordered and displaced from the trimer apex to the sides of the trimer and the V3 base fully exposed with the remainder of V3 disordered (PDB code 6U0L). Regions that were buried in a closed Env conformation (left) but exposed in the sCD4-bound open conformation (right) are indicated by green shading inside a dotted black oval.

changes, including the insertion of the gp41 N-terminal fusion peptide into the host cell membrane and subsequent fusion of the viral and host cell membranes (1).

Soluble versions of HIV-1 Env ectodomains that were stabilized in a closed, prefusion conformation (SOSIP.664 trimers) (6) have been used to characterize interactions between antibodies and Env in the presence and absence of soluble CD4 (sCD4) (7), with the clade A BG505 SOSIP (6) and the clade B B41 SOSIP (8) being commonly used in structural studies. Structural characterizations using X-ray crystallography or single-particle cryo-electron microscopy (cryo-EM) depicted different conformational states (Fig. 1), including (i) a closed, prefusion state in which the gp120 V1V2 region is positioned at the trimer apex, shielding the V3 loop and the coreceptor binding site (7, 9–11), (ii) an "occluded open" state in which the trimer is open due to outward rotation of the gp120 protomers, but with no local structural rearrangements in the V1V2 and V3 regions with respect to the remainder of the gp120 subunit (12, 13), and (iii) a CD4-induced, fully open state in which the gp120 protomers rotate outwards with the V1V2 region displaced by ~40 Å to the sides of the trimer, exposing V3 and the coreceptor binding site (12, 14, 15).

HIV-1 Env is targeted by various types of antibodies, including rare broadly neutralizing antibodies (bNAbs) that neutralize multiple HIV-1 strains (16). Although the epitopes of bNAbs have been mapped to the closed, prefusion Env trimer (7) and an occluded-open Env conformation (12, 13), one class of antibodies, CD4-induced (CD4i) antibodies, recognize Env regions that are exposed as a result of Env conformational changes induced by CD4 binding (17). CD4i antibodies are not considered bNAbs because they are not very potent neutralizers, perhaps because their epitope is hidden on the ligand-free, closed-conformation trimer and/or because of the limited steric accessibility of the epitope when the viral Env is attached to CD4 on the host cell (18). However, because they bind to relatively conserved regions of gp120, these antibodies tend to recognize multiple HIV-1 strains (19–23) and can mediate antibody-dependent cellular cytotoxicity (ADCC) (24).

CD4i antibodies were initially structurally characterized as complexes of an antibody Fab bound to a monomeric gp120 core that contained truncations in the N and C termini, V1V2 and V3 loops, as first demonstrated in the structure of gp120 complexed with the CD4i antibody 17b and sCD4 (25). The CD4i epitopes on a monomeric gp120 core are located near the base of the V3 loop and the gp120 bridging sheet, a four-stranded anti-parallel β-sheet comprising the gp120 β20 and β21 strands and the β2 and β3 strands at the base of V1V2. The anti-parallel four-stranded bridging sheet (β20-β21-β2-β3) configuration was later observed in sCD4-bound, open-conformation SOSIP Env trimer structures (12, 14, 15, 26). However, the first closed-conformation SOSIP Env trimer structures showed a rearranged three-stranded bridging sheet in which the β2 and β3 gp120 strands switched positions from the four-stranded bridging sheet conformation to a three-stranded conformation in which β21 is parallel to the β3 strand and β2 adopts a helical conformation on the opposite side of β3 (9, 10). The three-stranded sheet conformation has subsequently been observed in Env trimer structures lacking bound sCD4 (7). Although an Env trimer-sCD4-coreceptor structure is not yet available, CD4i antibodies mimic host coreceptors in that they require conformational changes within Env for binding. Some CD4i antibodies, e.g., E51 and 412d, mimic the N-terminal residues of the CCR5 coreceptor by including sulfotyrosines in their heavy chain complementarity-determining region 3 (CDRH3) regions (15, 27, 28).

The gp120 V1V2 region induces antibodies in infected individuals (29), and results from the RV144 clinical vaccine trial indicated that antibody responses against the V1V2 region correlated inversely with the risk of infection (30, 31). Data from three additional human vaccine trials also suggested a role for V1V2 antibodies in reducing the risk of HIV infection (32–34). Multiple V1V2-specific antibodies have been isolated from HIV-1 donors (35). Structures of Env complexed with V1V2 bNAbs, e.g., CAP256-VRC26.25 (36, 37) and PG9 (38, 39), showed a single Fab binding to the apex of a closed Env trimer. Other antibodies that recognize the V1V2 region, V2i antibodies, e.g., 697D, 1361, 1393A, and 830A, were isolated from HIV-infected human donors and recognize conformational epitopes on gp120 but not V2 peptides (40–44). These antibodies are primarily derived from the VH1-69 gene segment and exhibit weak cross-neutralizing activity against neutralization-sensitive pseudotyped viruses (40–44). Given that the monomeric gp120 core in gp120-CD4i antibody complexes adopts the bridging sheet conformation found in the gp120s of open-conformation sCD4-Env trimer-CD4i antibody complexes (25), we investigated whether V2i monoclonal antibodies (MAbs) target the Env V1V2 region similarly to CD4i antibodies that recognize open-conformation Envs. Here, we present single-particle cryo-EM structures of V2i MAbs in complex with an sCD4-bound open SOSIP Env. For comparison, we also structurally characterized CG10, a CD4i antibody isolated from a gp120-sCD4-immunized mouse that was developed to characterize conformational rearrangements of gp120 associated with receptor binding (45, 46). Here, it is demonstrated that CG10 can directly engage both gp120 and CD4 in an open Env trimer-sCD4 complex. The structures demonstrate a variety of binding poses for these antibodies, all of which can be classified within the CD4i class of antibodies that recognize an sCD4-bound open Env trimer conformation.

RESULTS

Binding experiments demonstrate that V2i MAbs require sCD4 for recognizing Env trimer. To investigate whether V2i MAbs recognize closed or sCD4-bound open Envs, we evaluated binding of V2i antibody Fabs to either a ligand-free, closed B41 SOSIP Env trimer or a sCD4-bound open trimer. C-terminally tagged soluble SOSIP trimers were immobilized on an enzyme-linked immunosorbent assay (ELISA) plate using an anti-tag antibody, and the binding of a V2i Fab to trimer was subsequently detected in the presence or absence of sCD4 (Fig. 2A). As a positive control for CD4i antibody binding, we used a Fab from 17b, whose epitope is buried in a closed Env trimer but exposed in an open trimer and on gp120 monomers (12, 14, 25). As expected, 17b showed enhanced binding in the presence of sCD4 (Fig. 2B). The same behavior was observed for Fabs from V2i MAbs 1361, 1393A, 830A, and 697D (40–44);

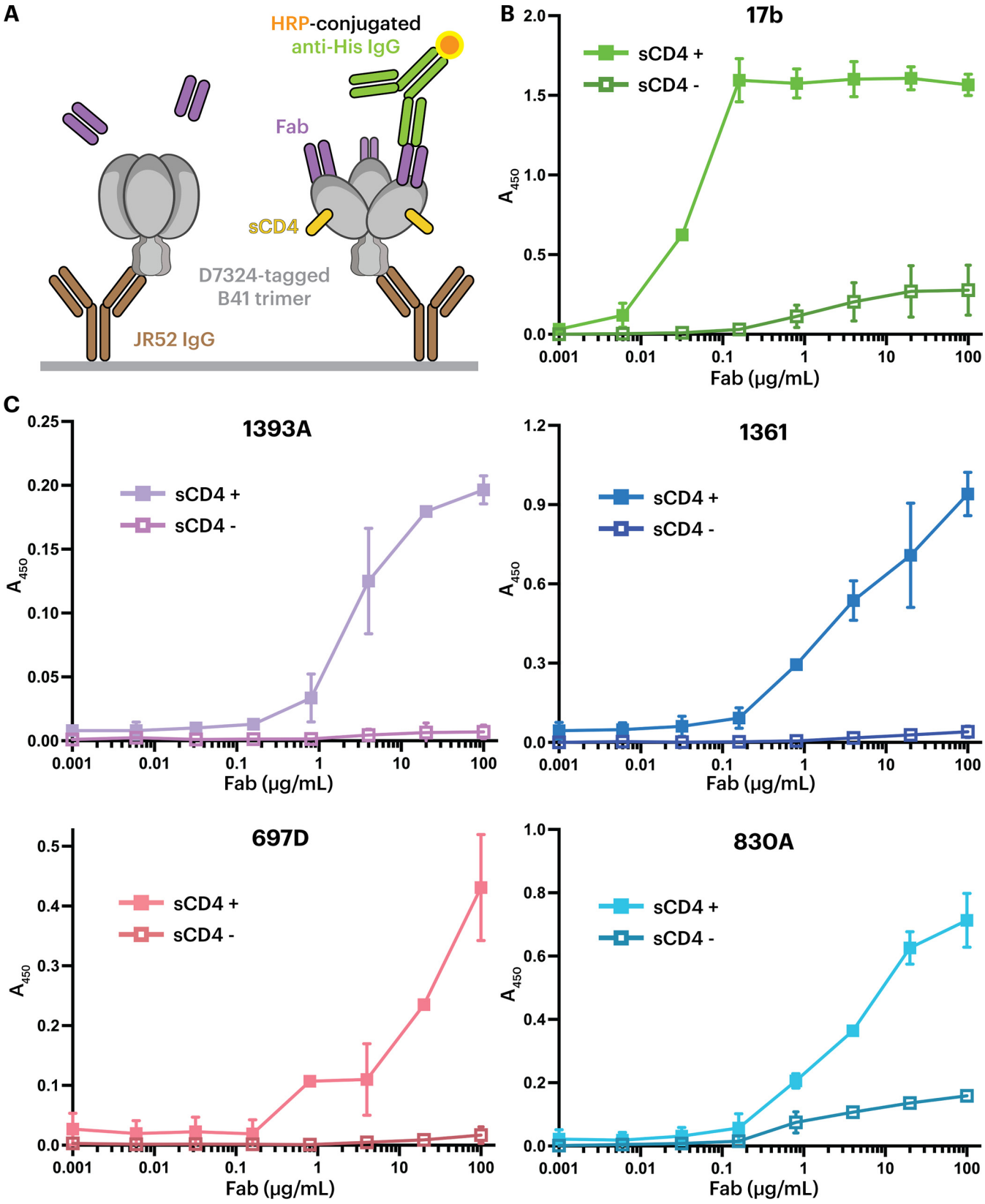

FIG 2 ELISAs demonstrate that V2i MAb Fabs preferentially recognize the sCD4-induced open conformation of B41 Env. (A) Schematic view of an ELISA in which D7324-tagged B41 SOSIP trimer was captured by the anti-D7324 antibody JR-52 (6), and V2i Fabs were added in the absence ($sCD4^-$, left) or presence ($sCD4^+$, right) of sCD4. (B) Positive control demonstrating preferential binding of the CD4i 17b Fab in the presence of sCD4. (C) Binding of the indicated V2i Fabs to B41 Env in the presence and absence of sCD4.

thus, maximal binding was observed in the presence of sCD4. These observations suggest that these V2i MAbs recognize the Env trimer similarly to CD4i antibodies, whereas anti-V1V2 bNAbs such as CAP256-VRC26.25 or PG9 recognize the closed Env conformation (36–39). In contrast to the other V2i antibodies, 830A exhibited weak binding to the sCD4-free, closed conformation trimer (Fig. 2C).

V2i MAbs bind to the CD4-induced open Env conformation. To further investigate the recognition mechanism of V2i MAbs, we structurally characterized V2i Fabs complexed with an sCD4-bound SOSIP trimer. We prepared complexes for single-particle cryo-EM by incubating a V2i Fab with SOSIP trimer and sCD4, initially starting with B41 Env trimers but switching to BG505 SOSIPs upon finding improvements in resolution for complexes with BG505. Structures of V2i Fab-BG505-sCD4 complexes were reconstructed to 7.5 Å, 6.1 Å, 7.0 Å, and 7.3 Å overall resolutions for Fabs 1393A, 1361, 697D, and 830A, respectively (see Fig. S1 and Table S1 in the supplemental material). Although these resolutions prohibited analyses of detailed side chain interactions, we could identify the polypeptide backbones and improve the quality of map densities at the Fab-gp120 interaction regions using local refinement methods (47, 48). To generate coordinates, we fitted the structure of an asymmetrically open BG505 Env trimer bound to sCD4 (PDB code 6U0L [15]) into the EM maps. To generate Fab coordinates, we used a crystal structure of 830A Fab (PDB code 4YWG) as a template (49), aligned its sequence to those of other V2i Fabs, replaced side chains that differed using polyalanine, and subsequently fit the Fab models into their respective EM maps.

Density maps of V2i Fab-BG505-sCD4 complexes showed that the Envs in all four structures adopted a fully open sCD4-bound Env conformation (12, 14, 15) in which the three gp120 protomers were rotated and displaced from the trimer 3-fold axis to expose the central region of Env and the V1V2 regions were displaced from the trimer apex to the sides of the Env to expose a largely disordered V3 region (Fig. 3). In all four V2i Fab-Env-sCD4 structures, the V2i Fab contacted the V1V2 region as well as the antiparallel β2 and β3 strands of the four-stranded bridging sheet (Fig. 3 and 4). Since these regions are not accessible in the closed prefusion or occluded-open Env conformations (Fig. 1), these V2i antibodies are predicted to recognize only the open, sCD4-bound conformation of Env.

Antibodies 1393A and 1361 approached the gp120 β2/β3 strands and the V1V2 regions nearly vertically from the apex of an open trimer, with their V_H-V_L domains facing downward (Fig. 3A, top). The angles of approach for 1393A and 1361 were comparable to those of CD4i Fabs such as 17b and E51, although the latter target the Env coreceptor binding site instead of its V1V2 region (12, 14, 15). Antibody 830A recognized a similar gp120 region yet approached the sides of the gp120 protomers, resulting in a nearly horizontal alignment of the antibody V_H-V_L and C_H-C_L domains (Fig. 3A, bottom), whereas antibody 697D approached the V1V2 region at an angle between that seen for the 1393A and 1361 antibodies and for antibody 830A (Fig. 3A, bottom). Finally, a portion of the V1V2 region (residues $Gln130_{gp120}$ to $Glu190_{gp120}$) that was disordered in structures of BG505 SOSIP and B41 SOSIP Env trimers bound to sCD4 and CD4i Fabs (e.g., 17b-B41-sCD4 [PDB code 5VN3] [12], 17b-BG505-sCD4-8ANC195 [PDB code 6CM3] [14], and E51-BG505-sCD4 [PDB code 6U0L] [15]) (Fig. 3B) was resolved in the structures involving the 1393A and 1361 Fabs (Fig. 3A). An ordered portion of V1V2 was also observed in the 21c-B41-sCD4-8ANC195 structure (PDB code 6EDU) in which the B41 V1V2 was stabilized by the 21c antibody light chain (14). For the 1393A- and 1361-Env complexes, the ordered portion of V1V2 was stabilized by the Fab heavy chains (Fig. 3B and 4).

Analysis of the structure of the 830A-BG505-sCD4 complex showed that the antibody bound to a side of the V1V2 region that could be partially accessed in a closed Env trimer (Fig. 4), rationalizing the ELISA results in which weak binding of 830A to an sCD4-free, closed-conformation trimer was detected (Fig. 2C).

To the limits of their respective resolutions, we found no detectable differences in epitopes recognized by V2i complexes with sCD4-bound BG505 or with B41 (data not

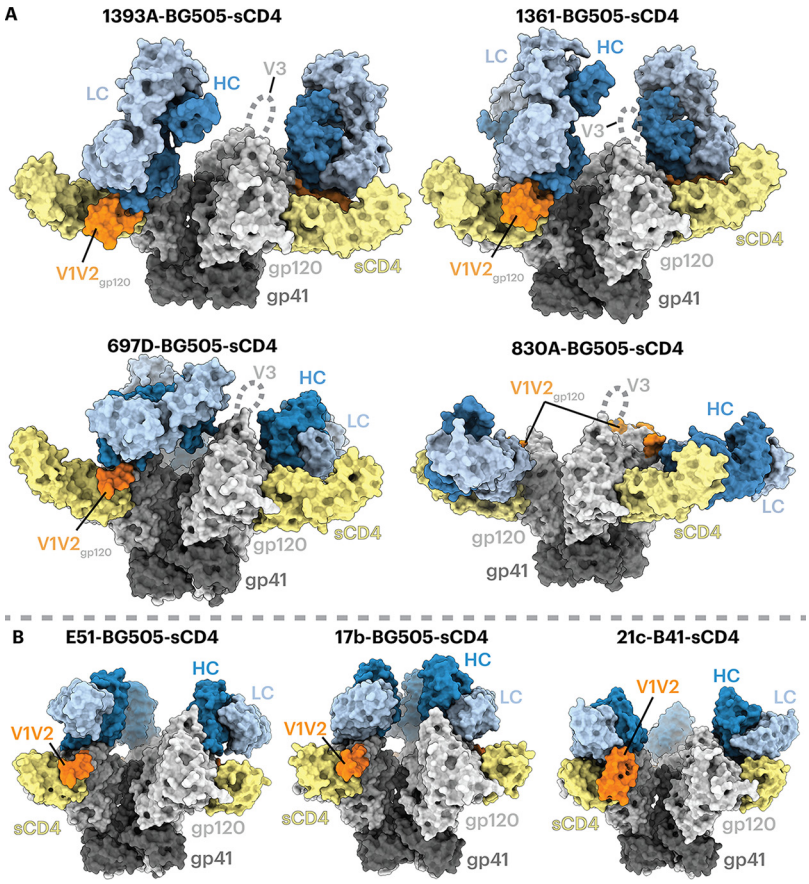

FIG 3 V2i Fabs adopt a variety of poses to recognize Env-sCD4. Fab heavy chains (HCs) are dark blue, light chains (LCs) are light blue, sCD4 is yellow, gp120 is light gray, gp41 is dark gray, and the ordered portion of gp120 V1V2 is orange. (A) Structures are shown as surface representations. A disordered V3 loop is indicated by dotted lines. (B) Surface depictions of previous CD4i Fab-Env-sCD4 complex structures: E51-BG505-sCD4 (PDB code 6U0L), 17b-BG505-sCD4-8ANC195 (PDB code 6CM3), and 21c-B41-sCD4-8ANC195 (PDB code 6EDU).

shown), consistent with similarities of the complexes of the CD4i antibody 17b with either sCD4-BG505 (14) or sCD4-B41 (12).

Comparison of Env trimer recognition by V2i antibodies and a stringent CD4i antibody. V2i antibodies elicited during natural HIV-1 infection that exhibited CD4i antibody characteristics were compared to CG10, a CD4i antibody that was elicited in a mouse immunized with a gp120-sCD4 complex (45). Unlike most other CD4i antibodies, CG10 was hypothesized to be strictly dependent on a CD4-induced conformation of gp120, typically the result of sCD4 binding (45, 46), as seen for prototype CD4i antibodies, such as 17b, that require sCD4 for binding to cell surface HIV-1 Env trimers (19) or to soluble BG505 SOSIP Env trimers (6). The requirement of sCD4 for 17b binding to Env is understood to reflect CD4-induced conformational changes, as the 17b Fab showed no direct contacts with sCD4 in crystal structures of 17b-gp120-sCD4 complexes or 17b-Env-sCD4 cryo-EM structures (12, 14, 25). In contrast, 21c, although described as a CD4-relaxed CD4i antibody that bound monomeric gp120s in the absence of sCD4, some (14), but not all (50), studies showed contacts with sCD4 as well as with gp120 in structures of both sCD4-gp120 monomer and sCD4-Env trimer complexes (14, 50). To compare sCD4 requirements for V2i and CD4i antibodies that recognize Env trimers, we solved a 4.1-Å cryo-EM structure of CG10 complexed with sCD4 and the clade B B41 SOSIP (Fig. 5A and Fig. S2) and a 1.4-Å crystal structure of CG10 Fab (Fig. 5B and Table S2) that was fit into the CG10-B41-sCD4 density (Fig. 5A and Table S3).

The crystal structure of unbound CG10 Fab showed ordered complementarity-

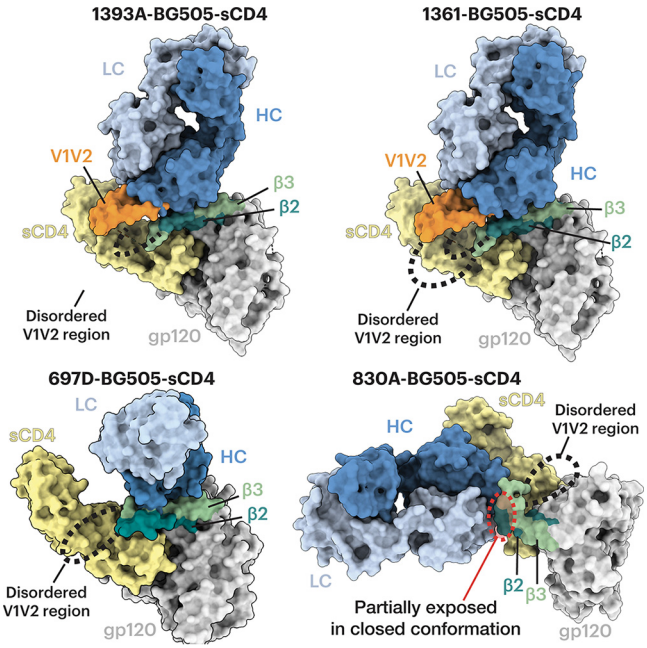

FIG 4 V2i Fabs contact gp120 β2, β3, and V1V2. Surface depictions of a gp120 monomer from the indicated Fab-trimeric Env-sCD4 structure are shown with the β2, β3, and V1V2 regions highlighted. Fab HCs are dark blue, LCs are light blue, sCD4 is yellow, gp120 is light gray, gp41 is dark gray, gp120 V1V2 is orange, the gp120 β2 and β3 strands are teal and green, respectively, and dashed lines indicate connections in V1V2 where density is missing in the EM maps. For the complexes with 1393A and 1361, a portion of V1V2 (orange) was stabilized by the Fab HC. (Bottom right) For the complex with V2i Fab 830A, the β2 and β3 strands were displaced and bent upwards, and the 830A epitope that is partially exposed in the closed Env conformation is highlighted in a red dashed oval.

determining regions (CDRs) on both the antibody heavy and light chains. Comparison of the V_H-V_L domains in the bound and unbound Fab structures showed that the conformational changes came mainly from the CDRH3 loop, while the rest of CDRs remained similar when bound to the sCD4-B41 complex (Fig. 5C) (root mean square deviation [RMSD] = ~1.5 Å for superimposition of 235 V_H-V_L Cα residues). The CG10-B41-sCD4 complex structure revealed an unusual interaction of the CG10 Fab CDRH3 with residues from both the B41 gp120 and sCD4 in which CDRH3 residue $Tyr97_{CG10\ HC}$ was sandwiched between positively charged residues on gp120 ($Lys432_{gp120}$) through a cation-π interaction and sCD4 ($Arg59_{sCD4}$) through a hydrogen bond (Fig. 5A). This architecture requires the existence of positively charged residues from both gp120 and sCD4 at their respective positions, likely explaining why CG10 was classified in the "stringent" class of CD4i antibodies (46). The specificity of this distinct interaction was demonstrated by binding experiments in which CG10 bound with higher affinity to gp120s from subtype B strains such as JR-FL and YU2, compared to a gp120 from subtype A strain BG505 (46), which can be explained by a lysine-to-glutamine substitution at BG505 residue 432_{gp120} that would disrupt the "sandwich" structure (Fig. 5A). Finally, the structure showed limited CG10 Fab contacts with the β2/β3 V1V2 strands that are displaced by sCD4 binding (12, 14, 15) (Fig. 5A), rationalizing previous observations demonstrating CG10 binding to gp120 cores with V1V2 truncations (46, 51).

DISCUSSION

The RV144 HIV-1 clinical vaccine trial showed a moderate but statistically significant decrease (31.2%) in risk of viral infection (52). In that study, a robust antibody response against the gp120 V1V2 region was inversely correlated with the risk of infection (30, 31, 53, 54). While vaccination trials such as RV144 using monomeric gp120 immunogens induced antibodies with cross-reactive profiles (30, 31), the antibodies elicited against epitopes exposed on monomeric gp120, but buried on a closed-conformation

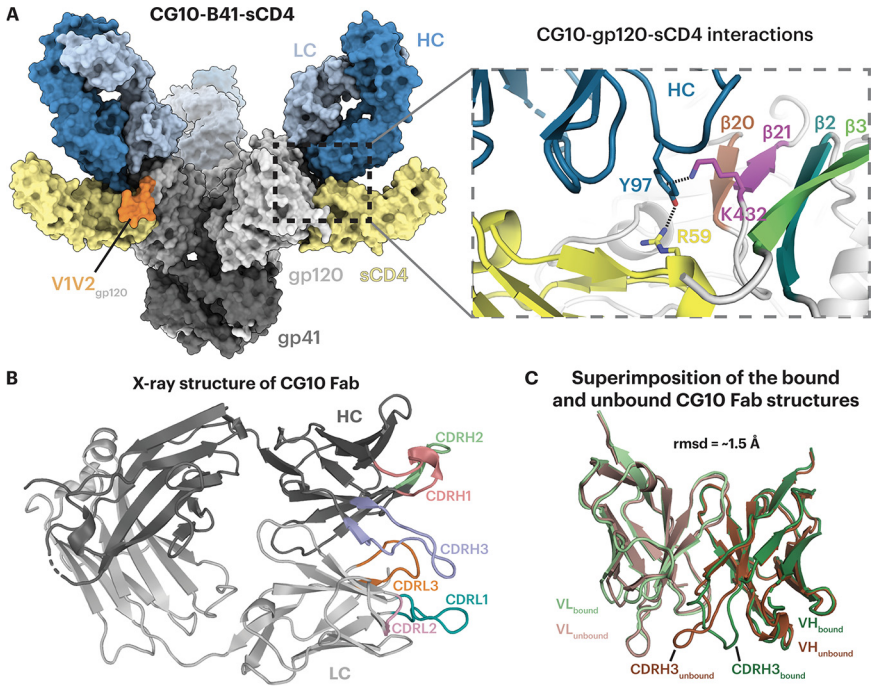

FIG 5 CG10 recognizes the CD4-induced open Env conformation and interacts with both sCD4 and gp120. (A) (Left) Surface representation of the cryo-EM structure of the CG10-B41-sCD4 complex. Env gp120 protomers are light gray, gp41 is dark gray, sCD4 is yellow, CG10 Fab HC and LC are dark and light blue, respectively, and V1V2 regions are orange. (Right) Close-up of CG10 residue $Tyr97_{HC}$ forming an interaction network with $Lys432_{gp120}$ and $Arg59_{CD4}$. The gp120 four-stranded bridging sheet is colored in brown, purple, teal, and green for the β20, β21, β2, and β3 strands, respectively. (B) X-ray structure of the CG10 Fab with colored CDR loops and HC and LC in dark and light gray, respectively. (C) Superimposition of the V_H-V_L domains of the unbound (dark and light brown for V_H and V_L, respectively) and bound (dark and light green) CG10 Fab.

Env trimer, have weak neutralizing activity compared to that of bNAbs that target the closed prefusion Env conformation. Nonetheless, the RV144-induced antibodies that target the V1V2 Env domain displayed antiviral activities, such as ADCC (55). How antibodies of this type can protect against viral infection has not yet been resolved; nonetheless, V1V2-specific antibodies have repeatedly been implicated in human trials as contributing to a reduced risk of HIV infection (31–34). To better understand the nature of these antibodies, we characterized four MAbs isolated from HIV-1-infected donors that target the V1V2 region of gp120 and that preferentially bind gp120 monomers rather than Env trimers (40–44). These V2i antibodies displayed little or no neutralizing activity *in vitro* in the absence of sCD4 but could mediate weak but detectable neutralization in the presence of sCD4 (56). They also mediated other antiviral activities, such as blocking of the binding of the $\alpha4\beta7$ integrin (a receptor on a subset of $CD4^+$ T cells that potentially facilitates HIV-1 seeding and replication in mucosae) (57–60), virus capture (61), and Fc-dependent antiviral effector functions (60).

Binding experiments suggested that the V2i antibodies preferentially recognized a CD4-bound open Env trimer conformation (Fig. 2C). Structural analysis using single-particle cryo-EM validated the binding results by showing that the V2i epitopes were inaccessible in the closed prefusion Env conformation (Fig. 3 and 4). Accordingly, these V2i antibodies can be categorized as CD4i MAbs that target the V1V2 region of sCD4-bound Env. For comparison, we also structurally characterized a CD4i antibody, CG10, that was isolated from a mouse that was immunized with a gp120-sCD4 complex for the purpose of revealing potential gp120 epitopes associated with CD4 binding (45, 46). An apparently CD4-induced epitope on gp120 monomers had been generated by gp120 binding to M2, a short peptide that bound gp120 without occluding the CD4 binding site (62). Thus, binding of CG10 to the gp120-M2 complex illustrates that CD4

itself is not absolutely required for CG10 binding to monomeric gp120. However, the structure of CG10-B41-sCD4, a complex of an Env trimer bound to both CG10 and sCD4, revealed a direct interaction between the antibody and sCD4, which further explains the reported stringency of the requirement for sCD4 for binding of CG10 to HIV-1 Env (45, 46) (Fig. 5A).

Unlike CG10, which was generated in response to recognition of an injected sCD4-gp120 complex (45), the V2i antibodies characterized in this study were isolated from HIV-1-infected donors, raising the question of how these antibodies were elicited since their epitopes are not completely accessible on closed, prefusion Env trimers (Fig. 1). Here, we propose two scenarios that could lead to the production of this type of antibody.

First, although cryo-electron tomography studies of Env conformations on HIV-1 virions show Env trimers in a closed, prefusion conformation (63–66), it is possible that ligand-free Env trimers can transiently adopt an open conformation that mimics a CD4-induced open conformation. This hypothesis is supported by studies of the dynamics of Env trimers showing structural changes occurring in the absence of CD4 that suggest that trimers can be in equilibrium between closed and more open conformations (67). Support for this model comes from biological studies. For example, studies focused on the Env V1V2 domain showed that the relative level of V2i MAb binding to Env-transfected cells increases with increasing time of exposure of cells to the MAb (56). The transient exposure of cryptic epitopes on unliganded trimers is further supported by data showing that V2i antibodies displayed an increased ability to neutralize virus if exposure of virus to V2i antibodies is extended beyond the 1-h incubation time typically used in *in vitro* neutralization experiments (56); this suggests that during the extended incubation period, epitopes occluded in the closed trimer become exposed for periods long enough to be recognized and bound by antibodies. These data, showing that unliganded trimers can undergo transient antigenic alterations, imply that they can also present transiently exposed epitopes as immunogenic determinants that can induce an immune response.

A second possibility is that V2i and other CD4i antibodies are elicited by CD4-gp120 complexes on target cells that form after gp120 is shed during fusion between the host and viral membranes, as suggested by electron tomography imaging of virus-host cells linked by prehairpin intermediates trapped by fusion inhibitors (68) (Fig. 6). In this scenario, CD4 binding followed by coreceptor binding to Env induces trimer opening (Fig. 6A), formation of the prehairpin intermediate in which the Env fusion peptide is inserted into the host cell membrane (68), and shedding of gp120 protomers (Fig. 6B). This process would generate membrane-associated CD4-gp120 complexes that remain on the surface of the host cell after fusion (Fig. 6B), serving as antigens that could elicit V2i and CD4i antibodies, and could function as targets for Fc-dependent antiviral activities of V2i antibodies (60). In addition, misfolded and uncleaved Envs, as well as gp160 monomers or dimers, that could be found on the surface of virions or infected cells might also contribute to the generation of this type of antibody.

MATERIALS AND METHODS

Protein expression and purification. Native-like HIV-1 Env trimers SOSIP.664 (BG505 and B41-D7324) contained SOS mutations at positions A501C$_{gp120}$ and T605C$_{gp41}$, the IP mutation (I559P$_{gp41}$), an improved furin cleavage site (REKR to RRRRRR), and a truncation after gp41 residue 664 (6, 8). For BG505, an additional mutation was introduced to include a potential *N*-linked glycosylation site at residue 332$_{gp120}$ (T332N$_{gp120}$). For B41 including the D7324 tag (6), the GSAPTKAKRRVVQREKR tag sequence was added after residue 664 in the gp41 ectodomain. Both Env trimers were expressed in Expi293F cells as described previously (13, 14). Transfected cell supernatants were filtered and Env trimers were purified as described previously (13) by a 2G12 immunoaffinity column followed by size exclusion chromatography (SEC) using a Superose 6 16/600 column (Cytiva). B41 SOSIP.664 v4.2 (8) was expressed in CHO stable cell lines kindly provided by Al Cupo and John Moore (Weill Cornell Medical College) and purified as described for BG505 SOSIP trimers produced in Expi293F cells.

All Fabs and sCD4 proteins were expressed in Expi293F cells. Fab light chain and 6×His-tagged heavy chain expression vectors were cotransfected and purified by nickel-nitrilotriacetic acid (Ni-NTA) chromatography followed by Superdex 200 Increase 10/300 GL column (Cytiva) SEC as previously described (13). The sCD4 expression vector encoded the D1D2 subunits of sCD4 (D1D2 domain residues

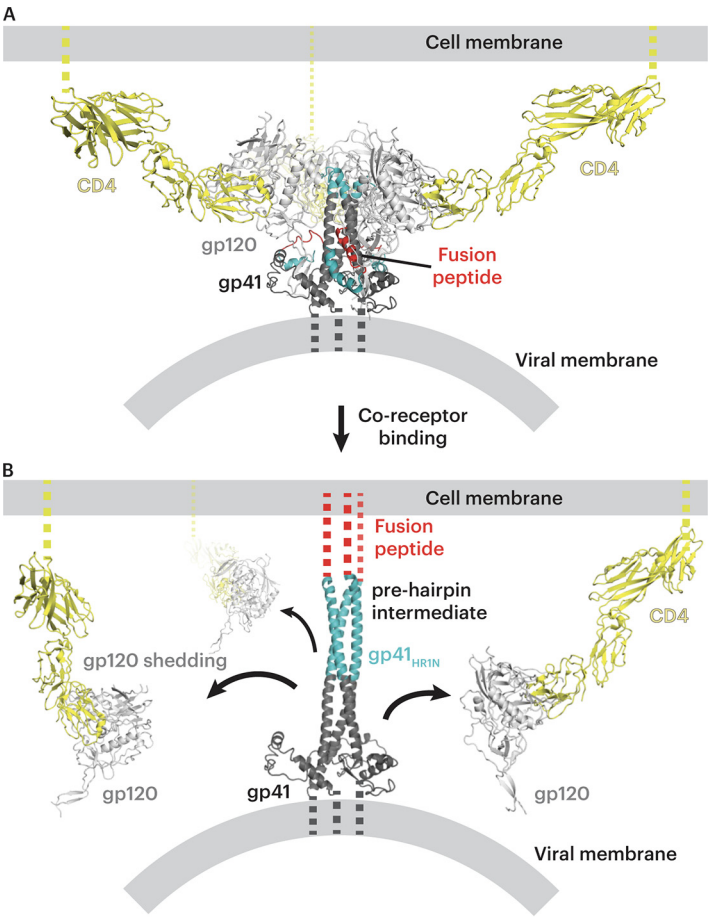

FIG 6 Model of postinfection formation of CD4-gp120 complexes on the host cell. (A) Open-conformation Env trimer (light and dark gray with fusion peptide in red and the N terminus of gp41 in cyan) on a viral membrane after binding to the host cell CD4 (yellow) on the host membrane. (B) Model of the prehairpin intermediate structure linking the viral and host cell membranes that is formed after host cell coreceptor binding (68). As potential targets to elicit V2i and CD4i antibodies during HIV-1 infection, cell surface CD4-gp120 complexes formed after gp120 shedding (black arrows) are shown on the host cell membrane.

1 to 186) followed by a Strep II Tag. sCD4 protein was purified by StrepTrap HP affinity columns (Cytiva) followed by SEC using a Superdex 200 Increase 10/300 GL column (Cytiva).

ELISA for MAb binding of CD4-induced Env. ELISAs were conducted by coating Corning Costar 96-well assay high binding plates (07-200-39) with the JR-52 MAb (kind gift of James Robinson, Tulane University), a mouse IgG that recognizes the D7324 tag (6), at 5 μg/mL in 0.1 M $NaHCO_3$ (pH 9.6) and incubating at 4°C overnight. Excess JR-52 MAb was removed and plates were blocked for 1 h at room temperature with 3% bovine serum albumin (BSA) in TBST (20 mM Tris, 150 mM NaCl, 0.1% Tween 20). Blocking buffer was removed and D7324-tagged B41 SOSIP was added at 5 μg/mL. After a 1-h incubation at room temperature, B41-D7324 was removed. For some experiments, sCD4 was added at 100 μg/mL and incubated for 2 h at room temperature. His-tagged Fabs were serially diluted with 3% BSA in TBST at a top concentration of 100 μg/mL and incubated for 2 h at room temperature. Fabs were removed and plates were washed twice with TBST. Mouse anti-His tag MAb conjugated with horseradish peroxidase (GenScript; A00186) at a 1:8,000 dilution was added and incubated for 30 min at room temperature. Plates were then washed 3 times with TBST. Colorimetric detection was accomplished using 1-Step Ultra TMB (3,3′,5,5′-tetramethylbenzidine)-ELISA substrate solution (Thermo Fisher Scientific; 34029), and color development was quenched with 1.0 N HCl. Absorption was measured at 450 nm. Two independent biological replicates for each ELISA were performed.

Cryo-EM sample preparation. V2i Fab-BG505-sCD4 and CG10-B41-sCD4 complexes were prepared by incubating purified and concentrated Fabs with soluble trimers and sCD4 at a molar ratio of 3.6:1:3.6 Fab/Env/sCD4 at room temperature for 4 h. A final concentration of 0.02% (wt/vol) fluorinated octylmaltoside (Anatrace) was added to samples before cryopreservation. Cryo-EM grids were prepared using a Mark IV Vitrobot (Thermo Fisher) operated at 12°C and 100% humidity. A 2.5-μL volume of concentrated sample was applied to 300-mesh Quantifoil R1.2/1.3 grids, incubated for 20 s, and blotted for 4 s, and grids were then plunge frozen in liquid ethane that was cooled by liquid nitrogen.

Cryo-EM data collection and processing. Cryo-grids were loaded onto a 300-kV Titan Krios electron microscope (Thermo Fisher) equipped with a GIF Quantum energy filter (slit width 20 eV) operating at a ×105,000 magnification (nominal). Defocus ranges for all complexes were set to 1.8 to 3.0 μm. Movies for 1393A, 1361, 697D, and 830A complexes were recorded with a 6k × 4k Gatan K3 direct electron detector operating in superresolution mode with pixel size of 0.416 Å·pixel^{-1} using SerialEM v3.7 software (69); movies for the CG10-BG505-sCD4 complex were recorded with a 4k × 4k Gatan K2 Summit direct electron detector operating in superresolution mode with a pixel size of 0.695 Å·pixel^{-1}. The recorded movies were sectioned into 40 subframes with dose rate of 1.5 e$-$/Å^2·subframe, generating a total dose of 60 e$-$·Å^2. Totals of 3,239 (1393A-BG505-sCD4), 2,412 (1361-BG505-sCD4), 2,340 (697D-BG505-sCD4), 1,872 (830A-BG505-sCD4), and 3,528 (CG10-B41-sCD4) movies were motion corrected using MotionCor2 (70) with 2× binning, and contrast transfer functions (CTFs) of the motion-corrected micrographs were calculated using CTFFIND v4.1.14 (71). Particles were automatically picked in cryoSPARC v3.2 (47) using the "Blob picker" program and classified using the "2D classification" program. Good 2D classes were selected for a second iteration of reference-free 2D classification. *Ab initio* models were generated and were subsequently refined with 3D refinements in cryoSPARC v3.2 (47, 48). 3D Fourier shell correlation (FSC) of maps was calculated using the remote 3DFSC processing server as described previously (72). The quality of EM map densities for Fab-gp120 interfaces was slightly improved using the cryoSPARC "Local refinement," in which particle alignments were focused on one protomer of a Fab-gp120-sCD4 complex (47, 48).

X-ray crystallography. Crystallization screens for CG10 Fab were carried out using the sitting drop vapor diffusion method at room temperature by mixing the Fab with an equal amount of screen solution (Hampton Research) using a TTP Labtech Mosquito automatic pipetting robot. CG10 Fab crystals were obtained in 14% (wt/vol) polyethylene glycol 4000 (PEG 4000)–0.1 M morpholineethanesulfonic acid (MES; pH 6.6) at room temperature. Crystals were looped and cryopreserved in liquid nitrogen.

X-ray diffraction data were collected using a Pilatus 6M detector (Dectris) at Stanford Synchrotron Radiation Lightsource (SSRL) beamline 12-2 at a wavelength of 1.0 Å. Data were indexed, integrated and scaled in XDS (73, 74), and merged with AIMLESS v0.7.4 (75). The CG10 Fab structure was determined by molecular replacement using PHASER v2.8.2 (76) using a mouse antibody with separated V_H-V_L and C_H-C_L domains as the search models (PDB code 4CMH). Coordinates of the Fab were refined using Phenix v1.19.2 (77, 78) and iterations of manual refinement using Coot v0.9 (79) (Table S1).

Model building. For V2i Fab-BG505-sCD4 complexes, coordinates for BG505 Env and sCD4 were fitted into the corresponding regions of density maps using an open-conformation BG505 trimer structure (PDB code 6U0L) (15). Coordinates for 830A Fab were fitted using the crystal structure of a 830A-gp120 complex (PDB code 4YWG) (49). For other V2i Fab coordinates (1393A, 1361, and 697D), residues that differed from those in 830A were replaced with polyalanines and fitted into their respective EM maps. For the CG10-B41-sCD4 cryo-EM complex, coordinates for CG10 Fab, B41 gp120 and gp41 subunits, and sCD4 were fitted into the corresponding regions of the EM density maps using the following coordinates for initial fitting: sCD4, gp120 and gp41 from an open-conformation B41 SOSIP (PDB code 5VN3) (12) and the unbound CG10 Fab (this study). Iterations of whole-complex refinements were carried out in Phenix (real space refine) (78) and manually done using Coot (79).

Structural analyses. Structural figures were made using PyMOL v2.5.1 (Schrödinger, LLC) or ChimeraX v1.2.5 (80). Interacting residues between CG10 Fab and B41-sCD4 were analyzed in PDBePISA (81) using the following definitions: potential hydrogen bonds were assigned using geometric criteria of an interatomic distance of $<$3.5 Å between the donor and acceptor residues and an A-D-H angle of $>$90°. Hydrogen atoms were added to proteins using PDB2PQR (82). The maximum distance allowed for van der Waals interaction was 4.0 Å. RMSDs were calculated for Cα atoms after superimposition in PyMOL v2.5.1 (Schrödinger, LLC) of the CG10 Fab from the CG10-B41-sCD4 complex and the unbound CG10 Fab X-ray structure.

Data availability. Cryo-EM maps generated in this study have been deposited in the Electron Microscopy Data Bank (EMDB) with accession codes EMD-27209, EMD-27210, EMD-27211, and EMD-27212 for V2i Fab complexes 1393A-BG505-sCD4, 1361-BG505-sCD4, 697D-BG505-sCD4, and 830A-BG505-sCD4, respectively. The cryo-EM map for CG10-B41-sCD4 complex was deposited in the EMDB under the accession code EMD-27208, and atomic model coordinates were deposited in the Protein Data Bank (PDB) under code 8D5C. The X-ray structure of CG10 Fab was deposited in the PDB under the code of 8D54.

SUPPLEMENTAL MATERIAL

Supplemental material is available online only.

SUPPLEMENTAL FILE 1, PDF file, 0.5 MB.

ACKNOWLEDGMENTS

We thank Jost Vielmetter at the Beckman Institute Protein Expression Center at Caltech for protein production, John Moore (Weill Cornell Medical College) for the B41 stable cell line, and James Robinson (Tulane University) for the JR-52 MAb. Cryo-EM studies were performed in the Beckman Institute Resource Center for Transmission Electron Microscopy at Caltech with assistance from S. Chen (director). We thank the Gordon and Betty Moore and Beckman Foundations for the gifts to Caltech to support the Molecular Observatory (Jens Kaiser, director) and the Stanford Synchrotron Radiation Lightsource (SSRL) beamline staff for data collection. Use of the SSRL, SLAC National Accelerator Laboratory, is supported

by the U.S. Department of Energy, Office of Science, Office of Basic Energy Sciences under contract no. DE-AC02-c76SF00515. The SSRL Structural Molecular Biology Program is supported by the DOE Office of Biological and Environmental Research and by the National Institutes of Health, National Institute of General Medical Sciences (P41GM103393). The contents of this publication are solely the responsibility of the authors and do not necessarily represent the official views of NIGMS or NIH.

This work was supported by grants from the National Institute of Allergy and Infectious Diseases (NIAID) (HIVRAD P01 AI100148 [P.J.B.], NIH P50 AI150464 [P.J.B.], and R01AI145655 [S.Z.-P.]), a Gates CAVD grant (INV-002143 [P.J.B.]), support from the Department of Medicine, Icahn School of Medicine at Mount Sinai (S.Z.-P.), and the generous support of Peter Kraus (J.M.G.).

Z.Y., K.-M.A.D., J.M.G., S.Z.-P., and P.J.B. designed the research. Z.Y. and K.-M.A.D. performed experiments and analyzed results. Z.Y., K.-M.A.D., and P.J.B. wrote the paper with input from coauthors.

We declare no competing interests.

REFERENCES

1. Harrison SC. 2015. Viral membrane fusion. Virology 479-480:498–507. https://doi.org/10.1016/j.virol.2015.03.043.
2. West AP, Scharf L, Scheid JF, Klein F, Bjorkman PJ, Nussenzweig MC. 2014. Structural insights on the role of antibodies in HIV-1 vaccine and therapy. Cell 156:633–648. https://doi.org/10.1016/j.cell.2014.01.052.
3. McCoy LE, Burton DR. 2017. Identification and specificity of broadly neutralizing antibodies against HIV. Immunol Rev 275:11–20. https://doi.org/10.1111/imr.12484.
4. Choe H, Farzan M, Sun Y, Sullivan N, Rollins B, Ponath PD, Wu L, Mackay CR, LaRosa G, Newman W, Gerard N, Gerard C, Sodroski J. 1996. The chemokine receptors CCR3 and CCR5 facilitate infection by primary HIV-1 isolates. Cell 85:1135–1148. https://doi.org/10.1016/s0092-8674(00)81313-6.
5. Feng Y, Broder CC, Kennedy PE, Berger EA. 1996. HIV-1 entry cofactor: functional cDNA cloning of a seven-transmembrane, G protein-coupled receptor. Science 272:872–877. https://doi.org/10.1126/science.272.5263.872.
6. Sanders RW, Derking R, Cupo A, Julien J-P, Yasmeen A, de Val N, Kim HJ, Blattner C, de la Peña AT, Korzun J, Golabek M, de los Reyes K, Ketas TJ, van Gils MJ, King CR, Wilson IA, Ward AB, Klasse PJ, Moore JP. 2013. A next-generation cleaved, soluble HIV-1 Env trimer, BG505 SOSIP.664 gp140, expresses multiple epitopes for broadly neutralizing but not non-neutralizing antibodies. PLoS Pathog 9:e1003618. https://doi.org/10.1371/journal.ppat.1003618.
7. Ward AB, Wilson IA. 2017. The HIV-1 envelope glycoprotein structure: nailing down a moving target. Immunol Rev 275:21–32. https://doi.org/10.1111/imr.12507.
8. Pugach P, Ozorowski G, Cupo A, Ringe R, Yasmeen A, de Val N, Derking R, Kim HJ, Korzun J, Golabek M, de los Reyes K, Ketas TJ, Julien J-P, Burton DR, Wilson IA, Sanders RW, Klasse PJ, Ward AB, Moore JP. 2015. A native-like SOSIP.664 trimer based on an HIV-1 subtype B *env* gene. J Virol 89:3380–3395. https://doi.org/10.1128/JVI.03473-14.
9. Julien J-P, Cupo A, Sok D, Stanfield RL, Lyumkis D, Deller MC, Klasse P-J, Burton DR, Sanders RW, Moore JP, Ward AB, Wilson IA. 2013. Crystal structure of a soluble cleaved HIV-1 envelope trimer. Science 342:1477–1483. https://doi.org/10.1126/science.1245625.
10. Lyumkis D, Julien J-P, de Val N, Cupo A, Potter CS, Klasse P-J, Burton DR, Sanders RW, Moore JP, Carragher B, Wilson IA, Ward AB. 2013. Cryo-EM structure of a fully glycosylated soluble cleaved HIV-1 envelope trimer. Science 342:1484–1490. https://doi.org/10.1126/science.1245627.
11. Gristick HB, von Boehmer L, West AP, Jr, Schamber M, Gazumyan A, Golijanin J, Seaman MS, Fätkenheuer G, Klein F, Nussenzweig MC, Bjorkman PJ. 2016. Natively glycosylated HIV-1 Env structure reveals new mode for antibody recognition of the CD4-binding site. Nat Struct Mol Biol 23:906–915. https://doi.org/10.1038/nsmb.3291.
12. Ozorowski G, Pallesen J, de Val N, Lyumkis D, Cottrell CA, Torres JL, Copps J, Stanfield RL, Cupo A, Pugach P, Moore JP, Wilson IA, Ward AB. 2017. Open and closed structures reveal allostery and pliability in the HIV-1 envelope spike. Nature 547:360–363. https://doi.org/10.1038/nature23010.
13. Yang Z, Dam K-MA, Bridges MD, Hoffmann MAG, DeLaitsch AT, Gristick HB, Escolano A, Gautam R, Martin MA, Nussenzweig MC, Hubbell WL, Bjorkman PJ. 2022. Neutralizing antibodies induced in immunized macaques recognize the CD4-binding site on an occluded-open HIV-1 envelope trimer. Nat Commun 13:732. https://doi.org/10.1038/s41467-022-28424-3.
14. Wang H, Barnes CO, Yang Z, Nussenzweig MC, Bjorkman PJ. 2018. Partially open HIV-1 envelope structures exhibit conformational changes relevant for coreceptor binding and fusion. Cell Host Microbe 24:579–592.e4. https://doi.org/10.1016/j.chom.2018.09.003.
15. Yang Z, Wang H, Liu AZ, Gristick HB, Bjorkman PJ. 2019. Asymmetric opening of HIV-1 Env bound to CD4 and a coreceptor-mimicking antibody. Nat Struct Mol Biol 26:1167–1175. https://doi.org/10.1038/s41594-019-0344-5.
16. Burton DR, Hangartner L. 2016. Broadly neutralizing antibodies to HIV and their role in vaccine design. Annu Rev Immunol 34:635–659. https://doi.org/10.1146/annurev-immunol-041015-055515.
17. DeVico A, Fouts T, Lewis GK, Gallo RC, Godfrey K, Charurat M, Harris I, Galmin L, Pal R. 2007. Antibodies to CD4-induced sites in HIV gp120 correlate with the control of SHIV challenge in macaques vaccinated with subunit immunogens. Proc Natl Acad Sci U S A 104:17477–17482. https://doi.org/10.1073/pnas.0707399104.
18. Labrijn AF, Poignard P, Raja A, Zwick MB, Delgado K, Franti M, Binley J, Vivona V, Grundner C, Huang C-C, Venturi M, Petropoulos CJ, Wrin T, Dimitrov DS, Robinson J, Kwong PD, Wyatt RT, Sodroski J, Burton DR. 2003. Access of antibody molecules to the conserved coreceptor binding site on glycoprotein gp120 is sterically restricted on primary human immunodeficiency virus type 1. J Virol 77:10557–10565. https://doi.org/10.1128/jvi.77.19.10557-10565.2003.
19. Thali M, Moore JP, Furman C, Charles M, Ho DD, Robinson J, Sodroski J. 1993. Characterization of conserved human immunodeficiency virus type 1 gp120 neutralization epitopes exposed upon gp120-CD4 binding. J Virol 67:3978–3988. https://doi.org/10.1128/JVI.67.7.3978-3988.1993.
20. Xiang S-H, Doka N, Choudhary RK, Sodroski J, Robinson JE. 2002. Characterization of CD4-induced epitopes on the HIV type 1 gp120 envelope glycoprotein recognized by neutralizing human monoclonal antibodies. AIDS Res Hum Retroviruses 18:1207–1217. https://doi.org/10.1089/08892220260387959.
21. Burton DR, Desrosiers RC, Doms RW, Koff WC, Kwong PD, Moore JP, Nabel GJ, Sodroski J, Wilson IA, Wyatt RT. 2004. HIV vaccine design and the neutralizing antibody problem. Nat Immunol 5:233–236. https://doi.org/10.1038/ni0304-233.
22. Decker JM, Bibollet-Ruche F, Wei X, Wang S, Levy DN, Wang W, Delaporte E, Peeters M, Derdeyn CA, Allen S, Hunter E, Saag MS, Hoxie JA, Hahn BH, Kwong PD, Robinson JE, Shaw GM. 2005. Antigenic conservation and immunogenicity of the HIV coreceptor binding site. J Exp Med 201:1407–1419. https://doi.org/10.1084/jem.20042510.
23. Lee S, Peden K, Dimitrov DS, Broder CC, Manischewitz J, Denisova G, Gershoni JM, Golding H. 1997. Enhancement of human immunodeficiency virus type 1 envelope-mediated fusion by a CD4-gp120 complex-specific monoclonal antibody. J Virol 71:6037–6043. https://doi.org/10.1128/JVI.71.8.6037-6043.1997.
24. Lewis G, Finzi A, DeVico A, Pazgier M. 2015. Conformational masking and receptor-dependent unmasking of highly conserved Env epitopes recognized by non-neutralizing antibodies that mediate potent ADCC against HIV-1. Viruses 7:5115–5132. https://doi.org/10.3390/v7092856.

25. Kwong PD, Wyatt R, Robinson J, Sweet RW, Sodroski J, Hendrickson WA. 1998. Structure of an HIV gp120 envelope glycoprotein in complex with the CD4 receptor and a neutralizing human antibody. Nature 393:648–659. https://doi.org/10.1038/31405.
26. Wang H, Cohen AA, Galimidi RP, Gristick HB, Jensen GJ, Bjorkman PJ. 2016. Cryo-EM structure of a CD4-bound open HIV-1 envelope trimer reveals structural rearrangements of the gp120 V1V2 loop. Proc Natl Acad Sci U S A 113:E7151–E7158. https://doi.org/10.1073/pnas.1615939113.
27. Farzan M, Mirzabekov T, Kolchinsky P, Wyatt R, Cayabyab M, Gerard NP, Gerard C, Sodroski J, Choe H. 1999. Tyrosine sulfation of the amino terminus of CCR5 facilitates HIV-1 entry. Cell 96:667–676. https://doi.org/10.1016/s0092-8674(00)80577-2.
28. Choe H, Li W, Wright PL, Vasilieva N, Venturi M, Huang C-C, Grundner C, Dorfman T, Zwick MB, Wang L, Rosenberg ES, Kwong PD, Burton DR, Robinson JE, Sodroski JG, Farzan M. 2003. Tyrosine sulfation of human antibodies contributes to recognition of the CCR5 binding region of HIV-1 gp120. Cell 114:161–170. https://doi.org/10.1016/s0092-8674(03)00508-7.
29. Liu L, Li L, Nanfack A, Mayr LM, Soni S, Kohutnicki A, Agyingi L, Wang X-H, Tuen M, Shao Y, Totrov M, Zolla-Pazner S, Kong X-P, Duerr R, Gorny MK. 2019. Anti-V2 antibody deficiency in individuals infected with HIV-1 in Cameroon. Virology 529:57–64. https://doi.org/10.1016/j.virol.2019.01.011.
30. Haynes BF, Gilbert PB, McElrath MJ, Zolla-Pazner S, Tomaras GD, Alam SM, Evans DT, Montefiori DC, Karnasuta C, Sutthent R, Liao H-X, DeVico AL, Lewis GK, Williams C, Pinter A, Fong Y, Janes H, DeCamp A, Huang Y, Rao M, Billings E, Karasavvas N, Robb ML, Ngauy V, de Souza MS, Paris R, Ferrari G, Bailer RT, Soderberg KA, Andrews C, Berman PW, Frahm N, De Rosa SC, Alpert MD, Yates NL, Shen X, Koup RA, Pitisuttithum P, Kaewkungwal J, Nitayaphan S, Rerks-Ngarm S, Michael NL, Kim JH. 2012. Immune-correlates analysis of an HIV-1 vaccine efficacy trial. N Engl J Med 366:1275–1286. https://doi.org/10.1056/NEJMoa1113425.
31. Zolla-Pazner S, deCamp A, Gilbert PB, Williams C, Yates NL, Williams WT, Howington R, Fong Y, Morris DE, Soderberg KA, Irene C, Reichman C, Pinter A, Parks R, Pitisuttithum P, Kaewkungwal J, Rerks-Ngarm S, Nitayaphan S, Andrews C, O'Connell RJ, Yang Z-y, Nabel GJ, Kim JH, Michael NL, Montefiori DC, Liao H-X, Haynes BF, Tomaras GD. 2014. Vaccine-induced IgG antibodies to V1V2 regions of multiple HIV-1 subtypes correlate with decreased risk of HIV-1 infection. PLoS One 9:e87572. https://doi.org/10.1371/journal.pone.0087572.
32. Fong Y, Shen X, Ashley VC, Deal A, Seaton KE, Yu C, Grant SP, Ferrari G, deCamp AC, Bailer RT, Koup RA, Montefiori D, Haynes BF, Sarzotti-Kelsoe M, Graham BS, Carpp LN, Hammer SM, Sobieszczyk M, Karuna S, Swann E, DeJesus E, Mulligan M, Frank I, Buchbinder S, Novak RM, McElrath MJ, Kalams S, Keefer M, Frahm NA, Janes HE, Gilbert PB, Tomaras GD. 2018. Modification of the association between T-cell immune responses and human immunodeficiency virus type 1 infection risk by vaccine-induced antibody responses in the HVTN 505 trial. J Infect Dis 217:1280–1288. https://doi.org/10.1093/infdis/jiy008.
33. Moodie Z, Dintwe O, Sawant S, Grove D, Huang Y, Janes H, Heptinstall J, Omar FL, Cohen K, De Rosa SC, Zhang L, Yates NL, Sarzotti-Kelsoe M, Seaton KE, Laher F, Bekker LG, Malahleha M, Innes C, Kassim S, Naicker N, Govender V, Sebe M, Singh N, Kotze P, Lazarus E, Nchabeleng M, Ward AM, Brumskine W, Dubula T, Randhawa AK, Grunenberg N, Hural J, Kee JJ, Benkeser D, Jin Y, Carpp LN, Allen M, D'Souza P, Tartaglia J, DiazGranados CA, Koutsoukos M, Gilbert PB, Kublin JG, Corey L, Andersen-Nissen E, Gray GE, Tomaras GD, McElrath MJ. 2022. Analysis of the HIV Vaccine Trials Network 702 phase 2b–3 HIV-1 vaccine trial in South Africa assessing RV144 antibody and T-cell correlates of HIV-1 acquisition risk. J Infect Dis 226:246–257. https://doi.org/10.1093/infdis/jiac260.
34. Kenny A, Luedtke A, Hyrien O, Fong Y, Burnham R, Heptinstall J, Sawant S, Stanfield-Oakley S, Omar FL, Khuzwayo S, Dintwe O, Borducchi E, Pattacini L, Willems W, Lavreys L, van Duijn J, Stieh DJ, Tomaka F, Pau MG, Gray GE, Buchbinder S, Mngadi K, McElrath MJ, Corey L, Barouch DH, De Rosa SC, Ferrari G, Andersen-Nissen E, Tomaras G, Gilbert PB. 2022. Immune correlates analysis of the Imbokodo HIV-1 vaccine efficacy trial. https://programme.aids2022.org/Abstract/Abstract/?abstractid=12669.
35. Sok D, Burton DR. 2018. Recent progress in broadly neutralizing antibodies to HIV. Nat Immunol 19:1179–1188. https://doi.org/10.1038/s41590-018-0235-7.
36. Doria-Rose NA, Bhiman JN, Roark RS, Schramm CA, Gorman J, Chuang G-Y, Pancera M, Cale EM, Ernandes MJ, Louder MK, Asokan M, Bailer RT, Druz A, Fraschilla IR, Garrett NJ, Jarosinski M, Lynch RM, McKee K, O'Dell S, Pegu A, Schmidt SD, Staupe RP, Sutton MS, Wang K, Wibmer CK, Haynes BF, Abdool-Karim S, Shapiro L, Kwong PD, Moore PL, Morris L, Mascola JR. 2016. New member of the V1V2-directed CAP256-VRC26 lineage that shows increased breadth and exceptional potency. J Virol 90:76–91. https://doi.org/10.1128/JVI.01791-15.
37. Gorman J, Chuang G-Y, Lai Y-T, Shen C-H, Boyington JC, Druz A, Geng H, Louder MK, McKee K, Rawi R, Verardi R, Yang Y, Zhang B, Doria-Rose NA, Lin B, Moore PL, Morris L, Shapiro L, Mascola JR, Kwong PD. 2020. Structure of super-potent antibody CAP256-VRC26.25 in complex with HIV-1 envelope reveals a combined mode of trimer-apex recognition. Cell Rep 31:107488. https://doi.org/10.1016/j.celrep.2020.03.052.
38. Wang H, Gristick HB, Scharf L, West AP, Galimidi RP, Seaman MS, Freund NT, Nussenzweig MC, Bjorkman PJ. 2017. Asymmetric recognition of HIV-1 envelope trimer by V1V2 loop-targeting antibodies. Elife 6:e27389. https://doi.org/10.7554/eLife.27389.
39. Walker LM, Phogat SK, Chan-Hui P-Y, Wagner D, Phung P, Goss JL, Wrin T, Simek MD, Fling S, Mitcham JL, Lehrman JK, Priddy FH, Olsen OA, Frey SM, Hammond PW, Kaminsky S, Zamb T, Moyle M, Koff WC, Poignard P, Burton DR, Protocol G Principal Investigators. 2009. Broad and potent neutralizing antibodies from an African donor reveal a new HIV-1 vaccine target. Science 326:285–289. https://doi.org/10.1126/science.1178746.
40. Gorny MK, Moore JP, Conley AJ, Karwowska S, Sodroski J, Williams C, Burda S, Boots LJ, Zolla-Pazner S. 1994. Human anti-V2 monoclonal antibody that neutralizes primary but not laboratory isolates of human immunodeficiency virus type 1. J Virol 68:8312–8320. https://doi.org/10.1128/JVI.68.12.8312-8320.1994.
41. Gorny MK, VanCott TC, Williams C, Revesz K, Zolla-Pazner S. 2000. Effects of oligomerization on the epitopes of the human immunodeficiency virus type 1 envelope glycoproteins. Virology 267:220–228. https://doi.org/10.1006/viro.1999.0095.
42. Nyambi PN, Mbah HA, Burda S, Williams C, Gorny MK, Nádas A, Zolla-Pazner S. 2000. Conserved and exposed epitopes on intact, native, primary human immunodeficiency virus type 1 virions of group M. J Virol 74:7096–7107. https://doi.org/10.1128/JVI.74.15.7096-7107.2000.
43. Pinter A, Honnen WJ, He Y, Gorny MK, Zolla-Pazner S, Kayman SC. 2004. The V1/V2 domain of gp120 is a global regulator of the sensitivity of primary human immunodeficiency virus type 1 isolates to neutralization by antibodies commonly induced upon infection. J Virol 78:5205–5215. https://doi.org/10.1128/jvi.78.10.5205-5215.2004.
44. Gorny MK, Pan R, Williams C, Wang X-H, Volsky B, O'Neal T, Spurrier B, Sampson JM, Li L, Seaman MS, Kong X-P, Zolla-Pazner S. 2012. Functional and immunochemical cross-reactivity of V2-specific monoclonal antibodies from HIV-1-infected individuals. Virology 427:198–207. https://doi.org/10.1016/j.virol.2012.02.003.
45. Gershoni JM, Denisova G, Raviv D, Smorodinsky NI, Buyaner D. 1993. HIV binding to its receptor creates specific epitopes for the CD4/gp120 complex. FASEB J 7:1185–1187. https://doi.org/10.1096/fasebj.7.12.7690724.
46. Kaplan G, Roitburd-Berman A, Lewis GK, Gershoni JM. 2016. Range of CD4-bound conformations of HIV-1 gp120, as defined using conditional CD4-induced antibodies. J Virol 90:4481–4493. https://doi.org/10.1128/JVI.03206-15.
47. Punjani A, Rubinstein JL, Fleet DJ, Brubaker MA. 2017. cryoSPARC: algorithms for rapid unsupervised cryo-EM structure determination. Nat Methods 14:290–296. https://doi.org/10.1038/nmeth.4169.
48. Punjani A, Zhang H, Fleet DJ. 2020. Non-uniform refinement: adaptive regularization improves single-particle cryo-EM reconstruction. Nat Methods 17:1214–1221. https://doi.org/10.1038/s41592-020-00990-8.
49. Pan R, Gorny MK, Zolla-Pazner S, Kong X-P. 2015. The V1V2 region of HIV-1 gp120 forms a five-stranded beta barrel. J Virol 89:8003–8010. https://doi.org/10.1128/JVI.00754-15.
50. Diskin R, Marcovecchio PM, Bjorkman PJ. 2010. Structure of a clade C HIV-1 gp120 bound to CD4 and CD4-induced antibody reveals anti-CD4 polyreactivity. Nat Struct Mol Biol 17:608–613. https://doi.org/10.1038/nsmb.1796.
51. Rizzuto CD, Wyatt R, Hernández-Ramos N, Sun Y, Kwong PD, Hendrickson WA, Sodroski J. 1998. A conserved HIV gp120 glycoprotein structure involved in chemokine receptor binding. Science 280:1949–1953. https://doi.org/10.1126/science.280.5371.1949.
52. Rerks-Ngarm S, Pitisuttithum P, Nitayaphan S, Kaewkungwal J, Chiu J, Paris R, Premsri N, Namwat C, de Souza M, Adams E, Benenson M, Gurunathan S, Tartaglia J, McNeil JG, Francis DP, Stablein D, Birx DL, Chunsuttiwat S, Khamboonruang C, Thongcharoen P, Robb ML, Michael NL, Kunasol P, Kim JH, MOPH-TAVEG Investigators. 2009. Vaccination with ALVAC and AIDSVAX to prevent HIV-1 infection in Thailand. N Engl J Med 361:2209–2220. https://doi.org/10.1056/NEJMoa0908492.
53. Zolla-Pazner S, deCamp AC, Cardozo T, Karasavvas N, Gottardo R, Williams C, Morris DE, Tomaras G, Rao M, Billings E, Berman P, Shen X, Andrews C, O'Connell RJ, Ngauy V, Nitayaphan S, de Souza M, Korber B, Koup R, Bailer RT,

Mascola JR, Pinter A, Montefiori D, Haynes BF, Robb ML, Rerks-Ngarm S, Michael NL, Gilbert PB, Kim JH. 2013. Analysis of V2 antibody responses induced in vaccinees in the ALVAC/AIDSVAX HIV-1 vaccine efficacy trial. PLoS One 8:e53629. https://doi.org/10.1371/journal.pone.0053629.
54. Zolla-Pazner S, Alvarez R, Kong X-P, Weiss S. 2019. Vaccine-induced V1V2-specific antibodies control and or protect against infection with HIV, SIV and SHIV. Curr Opin HIV AIDS 14:309–317. https://doi.org/10.1097/COH.0000000000000551.
55. Bonsignori M, Pollara J, Moody MA, Alpert MD, Chen X, Hwang K-K, Gilbert PB, Huang Y, Gurley TC, Kozink DM, Marshall DJ, Whitesides JF, Tsao C-Y, Kaewkungwal J, Nitayaphan S, Pitisuttithum P, Rerks-Ngarm S, Kim JH, Michael NL, Tomaras GD, Montefiori DC, Lewis GK, DeVico A, Evans DT, Ferrari G, Liao H-X, Haynes BF. 2012. Antibody-dependent cellular cytotoxicity-mediating antibodies from an HIV-1 vaccine efficacy trial target multiple epitopes and preferentially use the VH1 gene family. J Virol 86:11521–11532. https://doi.org/10.1128/JVI.01023-12.
56. Upadhyay C, Mayr LM, Zhang J, Kumar R, Gorny MK, Nádas A, Zolla-Pazner S, Hioe CE. 2014. Distinct mechanisms regulate exposure of neutralizing epitopes in the V2 and V3 loops of HIV-1 envelope. J Virol 88:12853–12865. https://doi.org/10.1128/JVI.02125-14.
57. Lertjuthaporn S, Cicala C, Van Ryk D, Liu M, Yolitz J, Wei D, Nawaz F, Doyle A, Horowitch B, Park C, Lu S, Lou Y, Wang S, Pan R, Jiang X, Villinger F, Byrareddy SN, Santangelo PJ, Morris L, Wibmer CK, Biris K, Mason RD, Gorman J, Hiatt J, Martinelli E, Roederer M, Fujikawa D, Gorini G, Franchini G, Arakelyan A, Ansari AA, Pattanapanyasat K, Kong X-P, Fauci AS, Arthos J. 2018. Select gp120 V2 domain specific antibodies derived from HIV and SIV infection and vaccination inhibit gp120 binding to $\alpha 4\beta 7$. PLoS Pathog 14:e1007278. https://doi.org/10.1371/journal.ppat.1007278.
58. Chung AW, Crispin M, Pritchard L, Robinson H, Gorny MK, Yu X, Bailey-Kellogg C, Ackerman ME, Scanlan C, Zolla-Pazner S, Alter G. 2014. Identification of antibody glycosylation structures that predict monoclonal antibody Fc-effector function. AIDS 28:2523–2530. https://doi.org/10.1097/QAD.0000000000000444.
59. Zolla-Pazner S, Powell R, Yahyaei S, Williams C, Jiang X, Li W, Lu S, Wang S, Upadhyay C, Hioe CE, Totrov M, Kong X. 2016. Rationally designed vaccines targeting the V2 region of HIV-1 gp120 induce a focused, cross-clade-reactive, biologically functional antibody response. J Virol 90:10993–11006. https://doi.org/10.1128/JVI.01403-16.
60. Musich T, Li L, Liu L, Zolla-Pazner S, Robert-Guroff M, Gorny MK. 2017. Monoclonal antibodies specific for the V2, V3, CD4-binding site, and gp41 of HIV-1 mediate phagocytosis in a dose-dependent manner. J Virol 91:e02325-16. https://doi.org/10.1128/JVI.02325-16.
61. Powell RL, Weiss S, Fox A, Liu X, Itri V, Jiang X, Luo CC, Spencer DA, Pandey S, Cheever T, Fuller DH, Totrov M, Hessell AJ, Haigwood NL, Kong X-P, Zolla-Pazner S. 2020. An HIV vaccine targeting the V2 region of the HIV envelope induces a highly durable polyfunctional Fc-mediated antibody response in rhesus macaques. J Virol 94:e01175-20. https://doi.org/10.1128/JVI.01175-20.
62. Roitburd-Berman A, Dela G, Kaplan G, Lewis GK, Gershoni JM. 2013. Allosteric induction of the CD4-bound conformation of HIV-1 Gp120. Retrovirology 10:147. https://doi.org/10.1186/1742-4690-10-147.
63. Liu J, Bartesaghi A, Borgnia MJ, Sapiro G, Subramaniam S. 2008. Molecular architecture of native HIV-1 gp120 trimers. Nature 455:109–113. https://doi.org/10.1038/nature07159.
64. Zhu P, Winkler H, Chertova E, Taylor KA, Roux KH. 2008. Cryoelectron tomography of HIV-1 envelope spikes: further evidence for tripod-like legs. PLoS Pathog 4:e1000203. https://doi.org/10.1371/journal.ppat.1000203.
65. Li Z, Li W, Lu M, Bess J, Chao CW, Gorman J, Terry DS, Zhang B, Zhou T, Blanchard SC, Kwong PD, Lifson JD, Mothes W, Liu J. 2020. Subnanometer structures of HIV-1 envelope trimers on aldrithiol-2-inactivated virus particles. Nat Struct Mol Biol 27:726–734. https://doi.org/10.1038/s41594-020-0452-2.
66. Mangala Prasad V, Leaman DP, Lovendahl KN, Croft JT, Benhaim MA, Hodge EA, Zwick MB, Lee KK. 2022. Cryo-ET of Env on intact HIV virions reveals structural variation and positioning on the Gag lattice. Cell 185:641–653.e17. https://doi.org/10.1016/j.cell.2022.01.013.
67. Hodge EA, Naika GS, Kephart SM, Nguyen A, Zhu R, Benhaim MA, Guo W, Moore JP, Hu S-L, Sanders RW, Lee KK. 2022. Structural dynamics reveal isolate-specific differences at neutralization epitopes on HIV Env. iScience 25:104449. https://doi.org/10.1016/j.isci.2022.104449.
68. Ladinsky MS, Gnanapragasam PN, Yang Z, West AP, Kay MS, Bjorkman PJ. 2020. Electron tomography visualization of HIV-1 fusion with target cells using fusion inhibitors to trap the pre-hairpin intermediate. Elife 9:e58411. https://doi.org/10.7554/eLife.58411.
69. Mastronarde DN. 2005. Automated electron microscope tomography using robust prediction of specimen movements. J Struct Biol 152:36–51. https://doi.org/10.1016/j.jsb.2005.07.007.
70. Zheng SQ, Palovcak E, Armache J-P, Verba KA, Cheng Y, Agard DA. 2017. MotionCor2: anisotropic correction of beam-induced motion for improved cryo-electron microscopy. Nat Methods 14:331–332. https://doi.org/10.1038/nmeth.4193.
71. Rohou A, Grigorieff N. 2015. CTFFIND4: fast and accurate defocus estimation from electron micrographs. J Struct Biol 192:216–221. https://doi.org/10.1016/j.jsb.2015.08.008.
72. Tan YZ, Baldwin PR, Davis JH, Williamson JR, Potter CS, Carragher B, Lyumkis D. 2017. Addressing preferred specimen orientation in single-particle cryo-EM through tilting. Nat Methods 14:793–796. https://doi.org/10.1038/nmeth.4347.
73. Kabsch W. 2010. *XDS*. Acta Crystallogr D Biol Crystallogr 66:125–132. https://doi.org/10.1107/S0907444909047337.
74. Kabsch W. 2010. Integration, scaling, space-group assignment and post-refinement. Acta Crystallogr D Biol Crystallogr 66:133–144. https://doi.org/10.1107/S0907444909047374.
75. Winn MD, Ballard CC, Cowtan KD, Dodson EJ, Emsley P, Evans PR, Keegan RM, Krissinel EB, Leslie AGW, McCoy A, McNicholas SJ, Murshudov GN, Pannu NS, Potterton EA, Powell HR, Read RJ, Vagin A, Wilson KS. 2011. Overview of the *CCP* 4 suite and current developments. Acta Crystallogr D Biol Crystallogr 67:235–242. https://doi.org/10.1107/S0907444910045749.
76. McCoy AJ, Grosse-Kunstleve RW, Adams PD, Winn MD, Storoni LC, Read RJ. 2007. *Phaser* crystallographic software. J Appl Crystallogr 40:658–674. https://doi.org/10.1107/S0021889807021206.
77. Adams PD, Afonine PV, Bunkóczi G, Chen VB, Davis IW, Echols N, Headd JJ, Hung L-W, Kapral GJ, Grosse-Kunstleve RW, McCoy AJ, Moriarty NW, Oeffner R, Read RJ, Richardson DC, Richardson JS, Terwilliger TC, Zwart PH. 2010. *PHENIX* : a comprehensive Python-based system for macromolecular structure solution. Acta Crystallogr D Biol Crystallogr 66:213–221. https://doi.org/10.1107/S0907444909052925.
78. Afonine PV, Poon BK, Read RJ, Sobolev OV, Terwilliger TC, Urzhumtsev A, Adams PD. 2018. Real-space refinement in *PHENIX* for cryo-EM and crystallography. Acta Crystallogr D Struct Biol 74:531–544. https://doi.org/10.1107/S2059798318006551.
79. Emsley P, Lohkamp B, Scott WG, Cowtan K. 2010. Features and development of *Coot*. Acta Crystallogr D Biol Crystallogr 66:486–501. https://doi.org/10.1107/S0907444910007493.
80. Goddard TD, Huang CC, Meng EC, Pettersen EF, Couch GS, Morris JH, Ferrin TE. 2018. UCSF ChimeraX: meeting modern challenges in visualization and analysis: UCSF ChimeraX visualization system. Protein Sci 27:14–25. https://doi.org/10.1002/pro.3235.
81. Krissinel E, Henrick K. 2007. Inference of macromolecular assemblies from crystalline state. J Mol Biol 372:774–797. https://doi.org/10.1016/j.jmb.2007.05.022.
82. Dolinsky TJ, Czodrowski P, Li H, Nielsen JE, Jensen JH, Klebe G, Baker NA. 2007. PDB2PQR: expanding and upgrading automated preparation of biomolecular structures for molecular simulations. Nucleic Acids Res 35:W522–W525. https://doi.org/10.1093/nar/gkm276.